Current Optics and Photonics
Vol. 2, No. 4, August 2018, pp. 348-355

ISSN: 2508-7266(Print) / ISSN: 2508-7274(Online)
DOI: https://doi.org/10.3807/COPP.2018.2.4.348

Creepage Distance Measurement Using Binocular Stereo Vision on Hot-line for High Voltage Insulator

Wenjun He*, Jiake Wang, and Yuegang Fu

School of Opto-electronic Engineering, Changchun University of Science and Technology, Changchun 130022, China

(Received November 6, 2017 : revised June 6, 2018 : accepted June 15, 2018)

How to measure the creepage distance of an insulator quickly and accurately is a problem for the power industry at present, and the noticeable concern is that the high voltage insulation equipment cannot be measured online in the charged state. In view of this situation, we develop an on-line measurement system of creepage distance for high voltage insulators based on binocular stereo vision. We have proposed a method of generating linear structured light using a conical off-axis mirror. The feasibility and effect of two ways to solve the interference problem of strong sunlight have been discussed, one way is to use bandpass filters to enhance the contrast ratio of linear structured light in the images, and the other way is to process the images with adaptive threshold segmentation and feature point extraction. After the system is calibrated, we tested the measurement error of the on-line measurement system with a composite insulator sample. Experimental results show that the maximum relative error is 1.45% and the average relative error is 0.69%, which satisfies the task requirement of not more than 5% of the maximum relative error.

Keywords : Optical devices, High voltage insulator, Binocular stereo vision, On-line measurement
OCIS codes : (120.4640) Optical instruments; (000.3110) Instruments, apparatus, and components common to the sciences

I. INTRODUCTION

High voltage insulators are widely used in electric power transmission engineering as electrical insulation components, and the umbrella skirts provide a major creepage distance for the high-voltage insulators [1]. As a result of long-term working in harsh climatic environments, the umbrella skirts of insulators are prone to aging deformation which is affected by high and low temperatures, snowstorms and other factors. The decrease of creepage distance will increase the probability of arc bridging between the umbrella skirts, and reduce the flashover voltage of the high voltage insulator, resulting in a pollution flashover accident that threatens the safe operation of the power grid [2-5]. Therefore, the periodic measurement of the pollution for high-voltage insulators is one of the important contents of the anti-pollution flashover work for the power grid system. And the parameters such as the diameter, surface area and creepage distance of the umbrella skirts are important indicators to characterize the pollution degree of the insulator. How to measure the creepage distance of the insulator quickly and accurately is a difficult problem for the power grid system at present, the biggest difficulty is that the high voltage insulation equipment cannot be measured online in the electrified state [6].

At present, the maintenance personnel of the power grid system mainly measure the creepage distance by tightly fitting the insulator surface with a flexible cord during a very short period of power outage, and the creepage distance is the sum of the outer contours of all the umbrella skirts [7]. This kind of manual measurement method has the disadvantages of low efficiency, huge workload and low accuracy. In order to solve this problem, Y. Liu proposed a photometric measurement method, using a single lens

*Corresponding author: hewenjun@cust.edu.cn, ORCID 0000-0001-8543-2694
Color versions of one or more of the figures in this paper are available online.

reflex camera with a laser bar generator to obtain the outer contour of the insulator, through the matching algorithm to obtain the creepage distance [8]. This measurement system with line-structured light is usually based on the laser triangulation method, mostly using 532 nm or 633 nm linear laser launcher. In the outdoor with strong sunlight, the visible light camera cannot get good images of insulator with line structured light [9], so it cannot effectively measure the creepage distance of high-voltage insulators. And this equipment can only be used indoors or on cloudy days.

In this paper, an on-line measurement system of creepage distance for high voltage insulator was developed based on binocular stereo vision, for the actual situation of insulators in a 110 kV substation. Two sets of zoom lenses were used to meet the measurement requirements for various types of insulators at different locations, and the interference problem caused by strong sunlight was effectively solved. Accurate and rapid measurement of creepage distance is of great significance for the power sector to estimate the cleaning period of insulators, to replace the damaged insulator equipment in a timely way, and to ensure the safety and reliability of power grid operation.

II. OPERATIONAL PRINCIPLE

2.1. Mathematical Model of Binocular Stereo Vision

The binocular stereo vision system usually collects the images of the same object by two cameras with different spatial positions to imitate the parallax of the human eye, and to extract the corresponding feature points in the image. By extracting the corresponding feature points in the images from the two cameras, the 2D coordinates of the two images are stereoscopically matched to form the 3D coordinates and to obtain the spatial coordinates of the object, so as to achieve some measurement functions, such as the measurement of distance and size, 3D reconstruction, target positioning and so on [10, 11]. The schematic diagram of the binocular stereo vision is shown in Fig. 1.

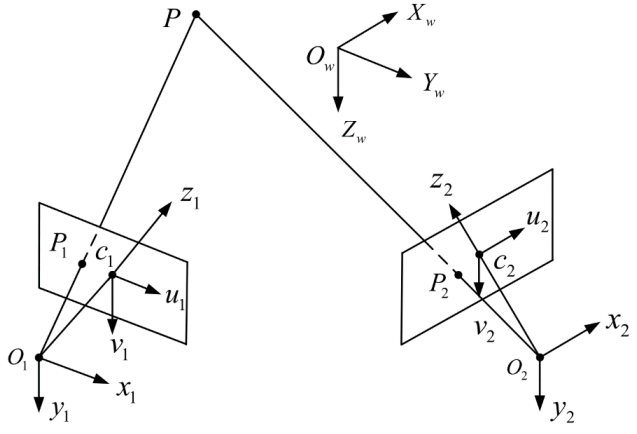

FIG. 1. Schematic diagram of the binocular stereo vision.

The imaging positions in the left and right camera's image plane of the point P which is described in the global coordinate system $O_w - X_w Y_w Z_w$ can be approximated by a pinhole imaging model. The local coordinate system of the left camera is $o_1 - x_1 y_1 z_1$ and its image coordinate system is $c_1 - u_1 v_1$, the projection point of P in the image plane is described as P_1. The perspective projection relationship between the object point P and the image point P_1 can be written as Eq. (1) [12, 13].

$$s\begin{pmatrix} u_1 \\ v_1 \\ 1 \end{pmatrix} = \begin{pmatrix} f_x & 0 & u_0 \\ 0 & f_y & v_0 \\ 0 & 0 & 1 \end{pmatrix} \begin{pmatrix} r_{11} & r_{12} & r_{13} & t_1 \\ r_{21} & r_{22} & r_{23} & t_2 \\ r_{31} & r_{32} & r_{33} & t_3 \end{pmatrix} \begin{pmatrix} X_w \\ Y_w \\ Z_w \\ 1 \end{pmatrix} \tag{1}$$

where s is a non-zero scale factor, $(u_1, v_1)^T$ is the local coordinate vector of the image point P_1, f_x and f_y represents the effective focal length of the left camera lens along the horizontal and vertical axes respectively, $(u_0, v_0)^T$ is the coordinate of the primary point of the left camera lens; $\mathbf{R}_L = (r_{ij})_{3\times3}$ is an orthogonal rotation matrix that converts the global coordinate system to the local coordinate system of the left camera, $\vec{t}_L = (t_x, t_y, t_z)^T$ is a translation vector that converts the origin point O_w of the global coordinate system to the local coordinate system of the left camera, $(X_w, Y_w, Z_w)^T$ is the coordinate vector of the object point P in the global coordinate system. f_x, f_y, u_0 , v_0 are the internal parameters of the left camera and can be obtained when the camera is calibrated.

When we calculate the global coordinate of the object point P in the case that the local coordinate vector of the image point P_1 is known, two equations can be obtained by simplifying Eq. (1),

$$\begin{cases} A_{L-1}X_w + B_{L-1}Y_w + C_{L-1}Z_w = D_{L-1} \\ A_{L-2}X_w + B_{L-2}Y_w + C_{L-2}Z_w = D_{L-2} \end{cases} \tag{2}$$

where

$$\begin{cases} A_{L-1} = f_x r_{11} - (u_1 - u_0) r_{31} \\ B_{L-1} = f_x r_{12} - (u_1 - u_0) r_{32} \\ C_{L-1} = f_x r_{13} - (u_1 - u_0) r_{33} \\ D_{L-1} = (u_1 - u_0) t_z - f_x t_x \end{cases}, \begin{cases} A_{L-2} = f_y r_{21} - (u_1 - u_0) r_{31} \\ B_{L-2} = f_y r_{22} - (u_1 - u_0) r_{32} \\ C_{L-2} = f_y r_{23} - (u_1 - u_0) r_{33} \\ D_{L-2} = (u_1 - u_0) t_z - f_y t_y \end{cases} \tag{3}$$

Similarly, the rotation matrix and the translation vector corresponding to the right camera and the global coordinate system are R_R and $\vec{t}_R$ respectively, and the local coordinate vector of the image point P_2 in the right camera is $(u_2, v_2)^T$, the perspective relationship between P_2 and P can be described as

$$\begin{cases} A_{R-1}X_w + B_{R-1}Y_w + C_{R-1}Z_w = D_{R-1} \\ A_{R-2}X_w + B_{R-2}Y_w + C_{R-2}Z_w = D_{R-2} \end{cases} \quad (4)$$

Then we can calculate the 3D coordinates of arbitrary object point P by using the least squares method to solve Eqs. (2) and (4).

2.2. The Composition of the Measurement System

In general, there are many different types of insulators in high-voltage substations, with large differences in size and working position from the ground. In this paper, two electric zoom lenses with the same parameters are used as the optical lens of the binocular stereo vision system, in order to meet the measurement of a variety of different types of insulators in a 110 kV substation. The zoom ratio of the zoom lens is 17×, the focal length is from 7.5 mm to 128 mm, the iris range is F/1.6 – F/16, and the zoom and focus actions are controlled by the DC motors and position sensors. The model number of the zoom lens is HD17X7.5A-YN1, which is a CCTV lens by the FUJIFILM company. As shown in Fig. 2, two complementary metal oxide semiconductor (CMOS) with the same parameters are fixed on the focal planes of the left and right zoom lenses, and the CMOSs transmit the collected images with insulators to the computer via the USB interface. The CMOSs have the image size of 1/2 inch, pixel size of 3.2 μm, a resolution of 2048 × 1536, which can meet the requirement to measure different kinds of insulators in the range of object distance from 10 m to 50 m. The separation distance of the two cameras is 300 mm, and the optical axes of these two cameras are parallel to the central axis. In addition, a linear structured light generator is added to

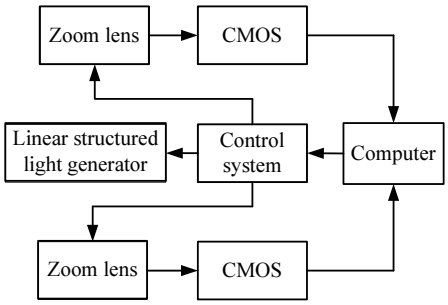

FIG. 2. Schematic diagram of the measurement system.

construct the feature points for binocular stereo vision measurement. It emits a laser line with an adjustable line width and irradiates the surface of the insulator to be measured. Adjustment of line width and synchronous zoom and focus of the electric zoom lenses are automatically controlled by the computer according to the calibrated object distance. When the measurement is started, the computer controls the two electric zoom lenses to simultaneously zoom and focus to find the appropriate image position. After adjusting the linear structured light generator, the laser line is hit with the finest line width at the insulator. The two CMOSs capture the images at the same time, and the feature points in the images can be automatically extracted by the adaptive threshold segmentation. The 3D coordinates of the feature points are acquired by stereo matching, and the creepage distance of the insulator can be obtained by calculating the spatial distance of the adjacent feature points. The photo of the measurement system is shown in Fig. 3.

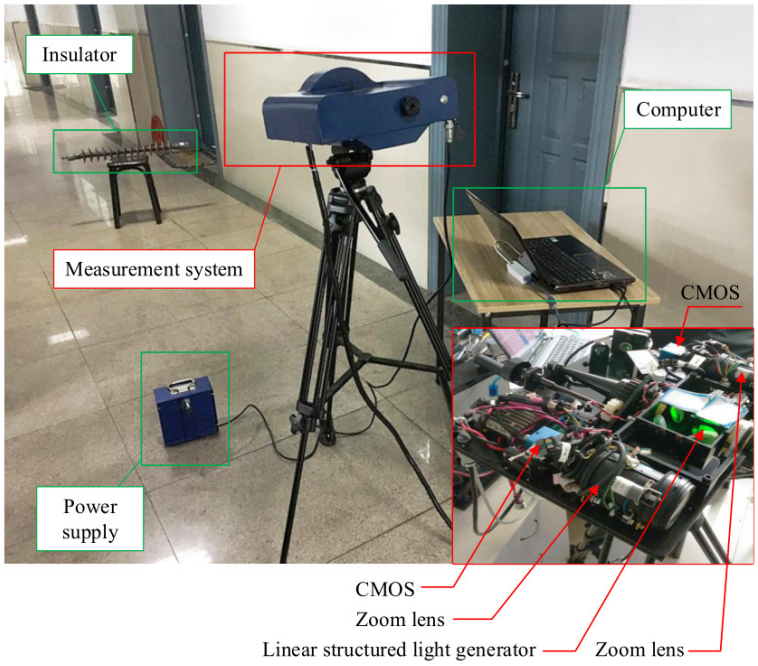

FIG. 3. Photo of the measurement system.

III. METHOD OF EXTRACTING THE FEATURE POINTS

3.1. Linear Structured Light Generator

It's a common method in binocular stereoscopic vision technology to use the linear structured light to provide the feature points of the left and right images for stereo matching. However, when measuring the creepage distance of the insulator, there are special requirements for the linear structured light: 1) The laser lines should have narrow linewidth within the projection distances of 10~50 m to achieve the precise extraction of feature points; 2) The entire laser line should be able to rotated 180° about the optical axis, so that the laser line can be aligned with the center of the insulator. In order to meet the above requirements, a set of linear structured light generators containing a zoom lens and an off-axis mirror with conical surface, is designed in this paper, and the schematic diagram of the linear structured light generator is shown in Fig. 4. The semiconductor laser has a wavelength of 532 nm, a power of 32 mW, an exit beam diameter of 1.5 mm, and a divergence angle of less than 1.2 mrad. The adjustable mirror makes the laser and the optical axis of the zoom lens coincide. By designing the parameters of the zoom lens, the laser beam is always focused to a minimum spot within a finite distance of 10 m to 50 m in the continuous zoom process. Mirrors 1~4 are planar reflectors and play the role of folding optical path. The key device for transforming the laser beam into a laser line is the conical mirror, which works with the zoom lens to produce a laser bar with adjustable linewidth. Mirrors 2~4 and the conical mirror as a whole that can be rotated 180° around the optical axis of the zoom lens, then the output laser line can also be rotated 180° around the optical axis, so as to align the insulators with different spatial posture.

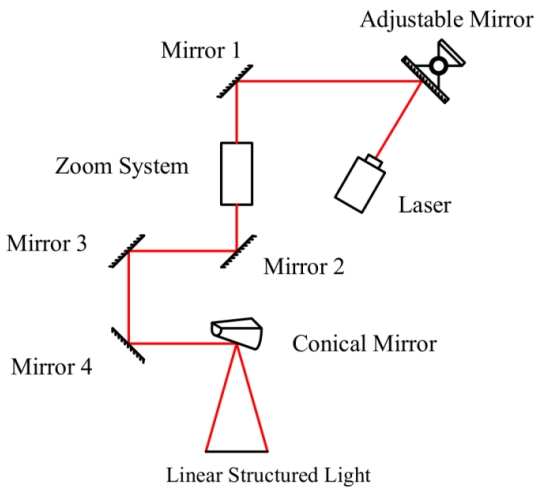

FIG. 4. Schematic diagram of linear structured light generator.

The zoom lens consists of two pairs of double glued lenses, and the laser beam can be focused continuously in the range of 10 m to 50 m by changing the interval between the two groups of glued lenses. The relationship between the width of the laser line and the projective distance is shown in Fig. 5, the laser linewidth is 0.91 mm at 10 m, and 3.68 mm at 50 m.

The off-axis mirror with conical surface can translate a circular laser beam into a linear laser bar, its working principle is shown in Fig. 6(a). When the parallel beam with the spot diameter D is incident at 45° along the z-axis to an off-axis conical mirror with a vertex angle of 90°, the reflected beam will exit along the y-axis, and the divergence angle in the z-axis direction will remain constant but in the x-axis direction will increase obviously. As shown in Fig. 6(a), ε represents the distance from the center of the incident beam to the optical axis of the conical mirror, d is the projection distance, L is the length of the laser bar in the distance of d, and the linewidth of the laser bar is equal to D.

$$L = (\frac{d}{\varepsilon} + 1)D \tag{5}$$

Due to the presence of the zoom lens, the laser beam which is incident on the off-axis conical mirror is not a strictly parallel beam, but a converging beam with a negative divergence angle. And the linewidth of the laser bar will be much smaller than D. Then the real length of the laser bar should be shorter than the calculated value of Eq. (5), and the modified formula as shown in Eq. (6).

$$L' = 2\tan\left(\arctan\left(\frac{D}{2\varepsilon}\right) - \arctan\left(\frac{D - D'}{2d}\right)\right)\cdot(d + \varepsilon) \tag{6}$$

where D' is the real linewidth of the laser bar at the projection distance.

In the actual measurement, the length of the laser bar is required to be not shorter than the length of the insulator. When the power of the laser is constant, the intensity of the laser bar is inversely proportional to the length of the laser bar. Therefore, it is necessary to design the distance from the center of the incident beam to the optical axis of

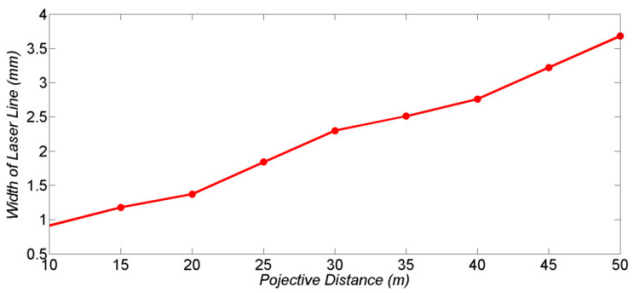

FIG. 5. Width of laser line VS projective distance.

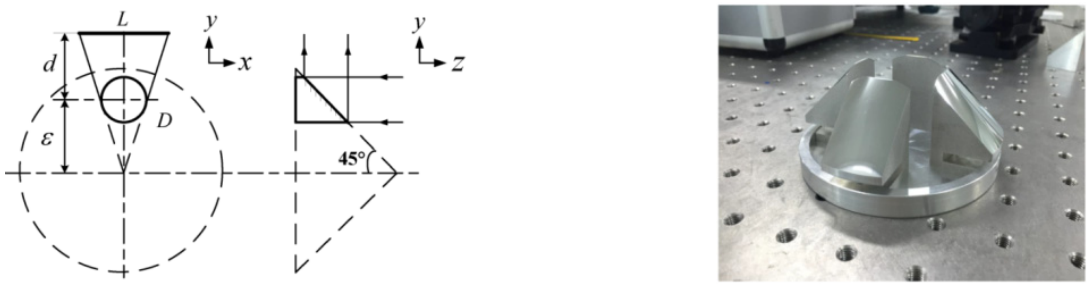

(a) (b)

FIG. 6. (a) Principle of the off-axis conical mirror, (b) Photo of the off-axis conical mirror.

the conical mirror according to the application requirements. In this paper, the off-axis conical mirror is manufactured with single point diamond turning technology, and the material is hard aluminum alloy, as shown in Fig. 6(b). The conic surface is a hyperbolic mirror with a conic constant of -2, and the off-axis distance is 48 mm.

3.2. Extraction of the Feature Points in a Strong Sunlight Environment

In the case of sunny weather, the intensity of outdoor sunlight at 532 nm is very strong, so it is very difficult to distinguish the laser bar from the insulator images. And it will seriously disturb the extraction of the feature points and the stereo matching for the binocular stereo vision, resulting in the measurement failing. In order to overcome the disturbance from the strong sunlight, we add a bandpass filter before the left CMOS, the effect is shown in Fig. 7. The bandpass filter has the center wavelength of 532 ± 0.6 nm, the full width half max (FWHM) of 3 ± 0.6 nm and cut-off depth of -40 dB. By comparing the bandpass filters with different parameters, we find that the bandpass filters with small FWHM have better effect to suppress the interference of the strong sunlight. However, if the FWHM is too small, the luminous flux to the CMOS will be significantly reduced, causing the exposure time to increase and the image frame rate to become too low. Therefore, the mechanical structures of the bandpass filters are designed to be quickly removable, and we choose bandpass filters with appropriate parameters according to the intensity of outdoor sunlight, there is no need to install bandpass filters when cloudy. The bandpass filters effectively enhance the contrast of the laser bar in the image, and making it easier to extract the feature points for stereo matching of the left and right images.

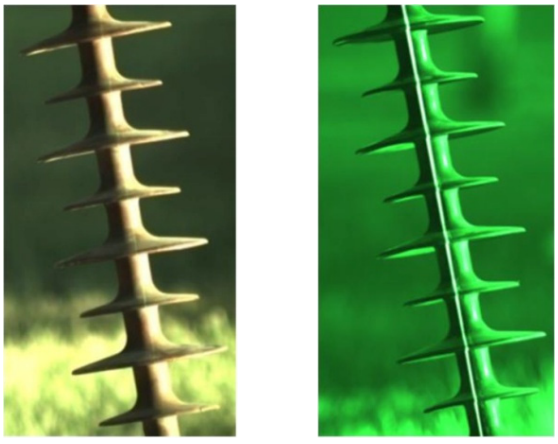

(a) (b)

FIG. 7. (a) Image without filter from right camera, (b) Image with filter from left camera.

As the measurement is in the outdoor environment, the backgrounds of the collected images are very complex. In order to separate the target from the background, we need to preprocess the images before extracting the feature points. Firstly, the images are transformed into gray scale images, the median filtering is performed, and then the adaptive threshold segmentation of gray images are realized based on an improved Otsu method [14]. The main purpose of the threshold segmentation is to obtain the initial region of the laser line with a high gray scale value, and to remove the reflection bright spots generated by the strong sunlight. Finally, the center line of the laser bar is extracted by using the gray centroid algorithm [15, 16]. When we take Fig. 7(b) as the initial image, and combine the improved Otsu method with the gray centroid algorithm to automatically extract the feature points in the image, the results are shown in Fig. 8. We can find that the traditional Otsu method is difficult to remove the bright spots which are caused by the reflection of sunlight, and the improved Otsu method can effectively distinguish the laser feature points from background.

For some models of high-voltage insulators, umbrella skirts have larger sizes and small interval. And it is difficult to measure the complete creepage distance of the insulator only at a certain angle, because the umbrella skirts will inevitably block each other. Therefore, we have two different angles to collect images, so that the left and right cameras respectively obtain two images. As shown as Figs. 9(a) and 9(b) are the images collected by the left and right cameras when the device is located on the right side of the insulator; Figs. 9(c) and 9(d) are the images collected by the left and right cameras when the device is located on the left side of the insulator.

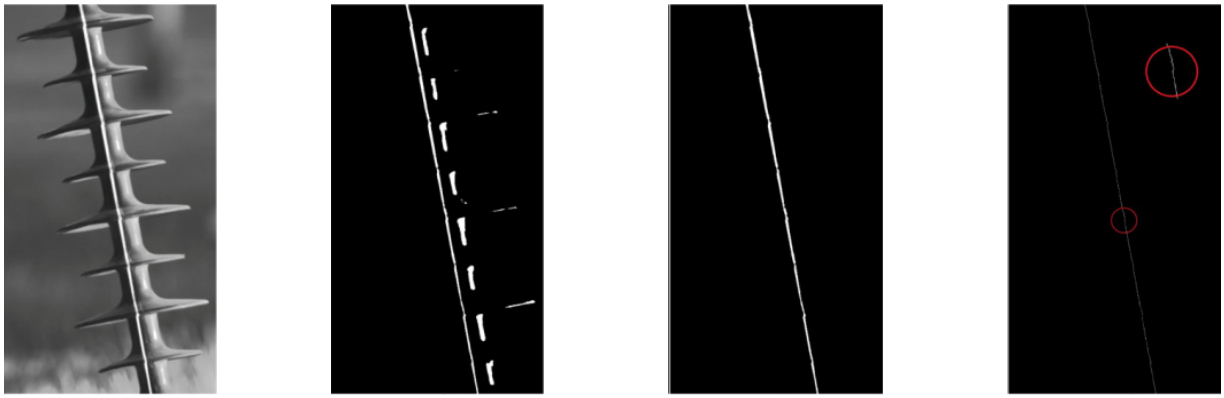

FIG. 8. (a) Grayscale of the original image, (b) Threshold segmentation result using Otsu method, (c) Threshold segmentation result using an improved Otsu method, (d) Extraction result of the center of the laser bar.

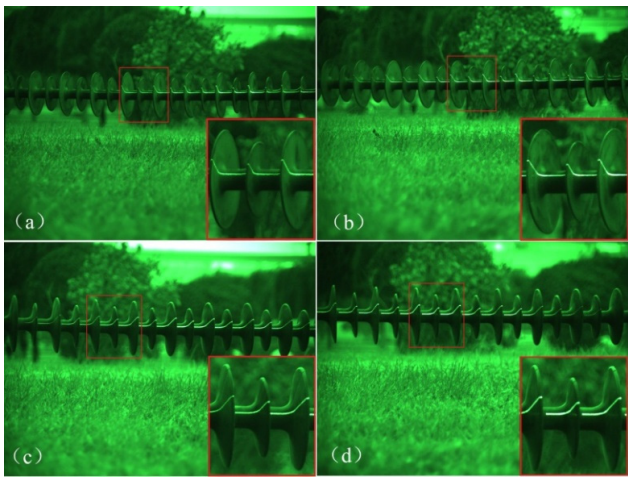

FIG. 9. Images collected by the left and right cameras at different angles.

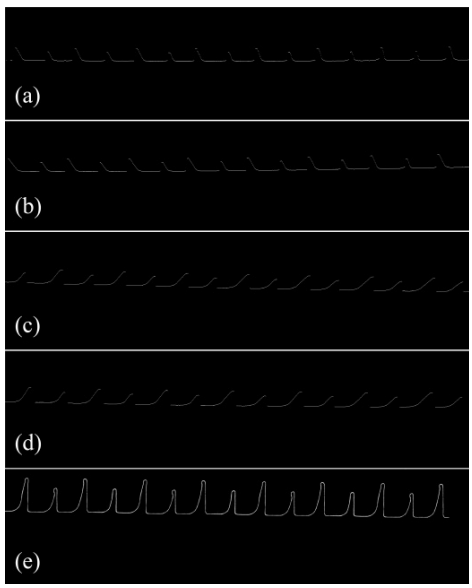

FIG. 10. Extraction results of the feature points.

The feature points of each image in Fig. 9 are extracted, and the results are shown in Figs. 10(a)~10(d). Then the graphs (a) and (b), (c) and (d) in Fig. 10 are respectively feature matched according to the scale-invariant feature transform (SIFT) algorithm [15]. When we get the corresponding feature point in the left and right images, the local coordinate vectors of object point P in the left and right cameras are obtained, and then the 3D global coordinates of object point P can be solved by using Eqs. (2)~(4). The 3D global coordinates of each feature point after the feature matching are calculated. However, the feature point clouds obtained by the feature matching from Figs. 10(a) and 10(b), or from Figs. 10(c) and 10(d) are incomplete, because the umbrella skirts of the insulator block each other. In order to solve this problem, we set an error threshold of the 3D global coordinates, and find the feature points with the same 3D global coordinates in the two feature point clouds based on the least squares method, then the two feature point clouds are combined into a complete feature point cloud. Using the line segment to connect the adjacent feature points to calculate the spatial distance between the adjacent points, and the sum of all segments is the creepage distance of the insulator, as shown in Fig. 10(e).

IV. SYSTEM CALIBRATION AND EXPERIMENT

According to the actual measurement requirements of 110 kV substation, seven groups of different focal lengths are set in the on-line measurement system, each group has 3 to 7 different focus positions, and there are 28 sets of optical parameters which ensure that all the insulators with in the distance of 10~50 m can be clearly imaged. The internal parameters and external parameters of the binocular stereo vision optical system are determined by using Zhang's calibration algorithm [17] to respectively calibrate the on-line measurement system with a different set of

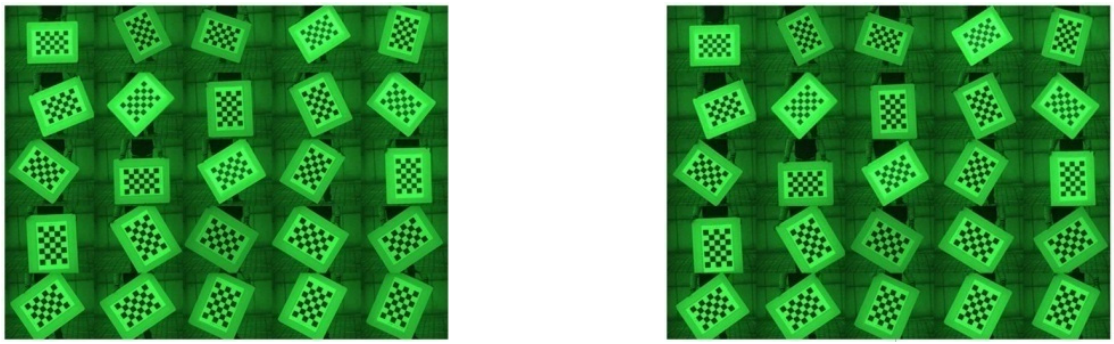

(a) (b)

FIG. 11 Camera calibration images: (a) for left camera, (b) for right camera.

optical parameters. As shown in Fig. 11, the left and right cameras simultaneously capture the images of the calibration plate in 25 different space postures, the calibration plate is a 5 × 7 checkerboard with a size of 90 mm × 90 mm for each grid.

In order to evaluate the measurement error of the on-line measurement system, a composite insulator sample with a creepage distance of 1580 mm was measured using this device. The two zoom lenses in front of the cameras were synchronously adjusted to the 7 groups of focal lengths when the system was calibrated, and the insulator was placed on different object distances which correspond to the focus positions. In other words, the measurement errors of the device with 28 sets of different optical parameters were tested, and the results are listed in Table 1.

For the same insulator, the measurement error is related to the focal length and the object distance, because the size of the insulator on the image plane is proportional to the ratio of the focal length to the object distance. As shown in Table 1, when the focal length is constant, the measurement error is positively correlated with the object distance. The maximum relative error is 1.45% and the average relative error is 0.69%, which satisfies the task requirement of not more than 5% of the maximum relative error. In the actual measurement, we should select an appropriate focal length according to the location and size of the insulator, so that the images of the insulator in the cameras can occupy a larger field of view. Then the actual size of the insulator represented by each pixel will be reduced, which will improve the measurement accuracy.

In order to verify the practicability of the device, we conducted an on-line testing experiment in the Sunjiazhai 110 kV substation, which is located in Qinghai Province, China, and the experimental scene is shown in Fig. 12. This on-line measurement device had experienced the test of the plateau climate and the low temperature in winter. And the insulators which were measured in the substation contained multiple types, such as suspension insulator, strain insulator, line post insulator, and station post insulator. The device in this paper achieves the on-line detection of the creepage distance for high-voltage insulators.

TABLE 1. Testing results of the creepage distance

No.	Focal length (mm)	Object distanc (m)	Creepage distance (mm)	Error (mm)	Relative error
1	30	10	1590.95	10.95	0.69%
2	30	12	1597.65	17.65	1.12%
3	30	14	1602.93	22.93	1.45%
4	41	10	1585.94	5.94	0.38%
5	41	13	1589.22	9.22	0.58%
6	41	16	1596.35	16.35	1.03%
7	52	10	1586.34	6.34	0.4%
8	52	13	1588.67	8.67	0.55%
9	52	16	1592.07	12.07	0.76%
10	52	19	1593.75	13.75	0.87%
11	70	15	1598.27	18.27	1.16%
12	70	18	1587.97	7.97	0.5%
13	70	21	1598.39	18.39	1.16%
14	89	14	1582.37	2.37	0.15%
15	89	18	1586.86	6.86	0.43%
16	89	21	1589.92	9.92	0.63%
17	89	24	1593.38	13.38	0.85%
18	108	18	1581.68	1.68	0.11%
19	108	20	1586.99	6.99	0.44%
20	108	24	1585.13	5.13	0.32%
21	108	28	1585.75	5.75	0.36%
22	126	28	1580.74	0.74	0.05%
23	126	32	1590.27	10.27	0.65%
24	126	36	1591.93	11.93	0.76%
25	126	40	1589.25	9.25	0.59%
26	126	44	1592.98	12.98	0.82%
27	126	48	1598.34	18.34	1.16%
28	126	50	1601.51	21.51	1.36%
AVG			1590.91	10.91	0.69%

FIG. 12. Experimental scene in the Sunjiazhai 110 kV substation which is located in Qinghai Province of China.

V. CONCLUSION

In conclusion, we have developed an on-line measurement system of creepage distance for high voltage insulators based on binocular stereo vision. The basic principles of the binocular stereo vision and the composition of the on-line measurement system have been shown in this paper. The method of generating the linear structured light using a conical off-axis mirror has been proposed. In order to solve the problem of interference caused by strong sunlight and complex background, we have used the bandpass fitters, and combined the improved Otsu method with the gray centroid algorithm to automatically extract the feature points in images. The experimental results show that the maximum relative error of the creepage distance is 1.45%, which has satisfied the requirement of the actual measurement task. At present, the system has been successfully applied to the on-line measurement of the creepage distance of insulators in Sunjiazhai 110 kV substation, which is located in Qinghai Province, China.

ACKNOWLEDGMENT

This study is supported by the National Natural Science Foundation of China (11474037), and the Science and Technology Development Project of Jilin Province (20160520015JH).

REFERENCES

1. R. Zhang, G. Wu, and T. Yuan, "Analysis on natural contamination characteristics of UHV AC post porcelain insulator," in *Proc. China International Conference on Electricity Distribution, IEEE* (Xi'an, China, Aug. 2016), pp. 16338584.
2. Z. Zhang, X. Jiang, Y. Chao, L. Chen, C. Sun, and J. Hu, "Study on DC pollution flashover performance of various types of long string insulators under low atmospheric pressure conditions," IEEE Trans. Power Del. **25**, 2132-2142 (2010).
3. Z. Zhang, D. Zhang, W. Zhang, C. Yang, X. Jiang, and J. Hu, "DC flashover performance of insulator string with fan-shaped non-uniform pollution," IEEE Trans. Dielectr. Electr. Insul. **22**, 177-184 (2015).
4. F. Zhang, L. Wang, Z. Guan, and M. Macalpine, "Influence of composite insulator shed design on contamination flashover performance at high altitudes," IEEE Trans. Dielectr. Electr. Insul. **18**, 739-744 (2011).
5. L. Shu, S. Wang, X. Jiang, Q. Hu, J. Liang, P. Yin, and J. Chen, "Modeling of AC flashover on ice-covered composite insulators with different shed configurations," IEEE Trans. Dielectr. Electr. Insul. **21**, 2642-2651 (2014).
6. Y. Ebisawa, S. Yamada, S. Mori, and T. Teranishi, "DC creepage breakdown characteristics of oil-immersed insulation," IEEE Trans. Dielectr. Electr. Insul. **16**, 1686-1692 (2009).
7. M. A. Salam and H. Ahmad, "Derivation of creepage distance in terms of ESDD and diameter of the contaminated insulator," IEEE Power Eng. Rev. **20**, 44-45 (2000).
8. L. Yawen, J. Jianwu, T. Min, Z. Ling, and W. Weijian, "Insulator creepage distance measurement based on photogrammetry method," Bull. Surv. Mapp. **12**, 15-17 (2012).
9. J. Zhen-yuan, F. Chao-nan, L. Wei, Y. Jing-hao, and X. Peng-tao, "Extraction of laser stripe centers based on equal matching points for binocular vision measurement," Opt. Precis. Eng. **24**, 1582-1591 (2016).
10. R. Anchini, C. Liguori, V. Paciello, and A. Paolillo, "A comparison between stereo-vision techniques for the reconstruction of 3-D coordinates of objects," IEEE Trans. Instrum. Meas. **55**, 1459-1466 (2006).
11. I. T. Comlekciler, S. Gunes, and C. Irgin, "Artificial 3-D contactless measurement in orthognathic surgery with binocular stereo vision," Appl. Soft Comput. **41**, 505-514 (2016).
12. J. Sun, H. Ma, and D. Zeng, "Three-dimensional infrared imaging method based on binocular stereo vision," Opt. Eng. **54**, 103111 (2015).
13. Z. Liu and T. Chen, "Distance measurement system based on binocular stereo vision," in *Proc. International Joint Conference on Artificial Intelligence. IEEE* (Hainan Island, China, April 2009), pp. 456-459.
14. J. Sa, X. Sun, T. Zhang, H. Li, and H. Zeng, "Improved Otsu segmentation based on sobel operator," in *Proc. International Conference on Systems and Informatics. IEEE* (Shanghai, China, Nov. 2016), pp. 886-890.
15. T. Lindeberg, "Image matching using generalized scale-space interest points," J. Math. Imaging Vis. **52**, 3-36 (2015).
16. T. Lindeberg, "Invariance of visual operations at the level of receptive fields," BMC Neurosci. **8**, 1-33 (2013).
17. Z. Zhang, "A flexible new technique for camera calibration," IEEE Trans. Pattern Anal. Mach. Intell. **22**, 1330-1334 (2000).